Niu et al. *Zool. Res.* 2026, 47(3): 835−850
https://doi.org/10.24272/j.issn.2095-8137.2025.191
https://cstr.cn/32248.14.zr.2025.191

ZR | Zoological Research

Article Open Access

CREBZF/c-Jun modulates ApoE-mediated cholesterol transport to influence female steroid hormone synthesis

Hong-Yu Niu[1,2], Chao Li[1,2], Rui-Hang Zhang[1,2], Mu-Zi Du[1], Ji-Ya Wuen[1], Hao-Kun Liu[1,2], Zu-Hui Li[1,2], Ai-Hua Wang[1,2], Ya-Ping Jin[1,2,*], Peng-Fei Lin[1,2,*]

[1] *College of Veterinary Medicine*, *Northwest A & F University*, *Yangling*, *Shaanxi* 712100, *China*

[2] *Key Laboratory of Animal Biotechnology*, *Ministry of Agriculture and Rural Affairs*, *Northwest A & F University*, *Yangling*, *Shaanxi* 712100, *China*

ABSTRACT

Ovarian secretion of steroid hormones is crucial for female reproductive health. CREBZF, a basic leucine zipper transcription factor, can heterodimerize with other transcription factors to regulate genes involved in various biological processes. This study investigates the role of CREBZF in female reproduction and steroid hormone synthesis regulation. Whole ovarian knockout of CREBZF affects the estrous cycle, antral follicle development, and testosterone and estradiol levels in female mice. Conditional knockout of CREBZF in Cyp17a1-positive cells results in altered serum testosterone during estrus, impaired postpartum maternal behavior, and significantly reduced offspring survival, associated with abnormal corticosterone and oxytocin levels. In NCI-H295R cells induced for steroidogenesis, CREBZF knockdown reduced testosterone and corticosterone secretion. RNA sequencing of CREBZF-knockdown NCI-H295R cells identified 51 differentially expressed genes enriched in steroidogenesis-related pathways. CREBZF knockdown also reduced c-Jun and ApoE expression, with a significant decrease in intracellular cholesterol. CREBZF interacts with c-Jun and binds to the ApoE promoter to regulate expression. Database screening identified two CREBZF/c-Jun binding sites, where CREBZF enhances c-Jun-mediated activation of ApoE at Site1 (–299 to –286 bp), but inhibits it at Site2 (+70 to +83 bp). In conclusion, the CREBZF/c-Jun complex regulates ApoE expression, influencing cholesterol levels and female steroidogenesis, which is crucial for reproductive function.

Keywords: CREBZF; Steroid hormones; Testosterone; Corticosterone; c-Jun; ApoE

INTRODUCTION

Steroidogenic disorders encompass a wide range of clinically significant conditions affecting gonadal and adrenal function, such as Congenital Adrenal Hyperplasia (CAH), Polycystic Ovary Syndrome (PCOS), Premature Ovarian Insufficiency (POI), and male hypogonadism, as well as other reproductive pathologies (Maher et al., 2023; Rosenfield, 2024; Touraine et al., 2024). These conditions not only compromise reproductive capacity but are also closely associated with systemic health issues, including metabolic syndrome and cardiovascular disease (Helvaci & Yildiz, 2025). Steroid hormones are classified into four major types: glucocorticoids, mineralocorticoids, sex hormones, and vitamin D (Payne & Hales, 2004). Despite structural differences, all steroid hormones are synthesized from cholesterol via a complex and tightly regulated process requiring the coordinated action of both ubiquitously and tissue-specifically expressed enzymes and regulatory factors (Miller & Auchus, 2011). In gonad, cholesterol is primarily derived from extracellular sources, delivered by lipoproteins containing apolipoproteins like Apolipoprotein A-I (ApoA-I), Apolipoprotein B-100 (ApoB-100), and Apolipoprotein E (ApoE), which interact with specific cell surface receptors such as Scavenger Receptor Class B Type 1 (SR-B1), Low-Density Lipoprotein Receptor (LDLR), and LDL Receptor-Related Protein 1 (LRP1) to facilitate cellular uptake(Dalhaimer et al., 2023). In the ovary, granulosa cells predominantly use the HDL-ApoA-SR-B1 pathway, while theca cells rely on the LDL-ApoE-LDLR/LRP1 pathway for cholesterol uptake to support androgen synthesis(Connelly & Williams, 2003; Oriá et al., 2020). Extensive research has identified a range of key enzymes and regulatory factors essential for steroidogenesis, such as the steroidogenic acute regulatory protein (StAR) and various members of the cytochrome P450 family (e.g., CYP11A1, CYP17A1). Mutations in these genes have been linked to various human diseases, underscoring their essential roles in steroid hormone biosynthesis (Miller, 2017). Nevertheless, the disease phenotypes and in vivo functions of apolipoproteins

Received: 11 October 2025; Accepted: 08 December 2025; Online: 09 December 2025

Foundation items: This work was supported by the National Natural Science Foundation of China (32172934)

*Corresponding authors, E-mail: linpengfei@nwsuaf.edu.cn; yapingjin@163.com

and potential novel regulators remain incompletely understood, and monogenic disorders associated with these factors have yet to be extensively investigated or modeled in animal systems.

CREBZF, a transcription factor belonging to the CREB/ATF protein family and characterized by a basic leucine zipper (bZIP) domain, exists in two isoforms: the long isoform (CREBZF-L), also known as Small Heterodimer Partner Interacting Leucine Zipper Protein (SMILE), and the short isoform (CREBZF-S), referred to as Zhangfei (Zf) (Xie et al., 2008). Although these isoforms are produced by alternative translation initiation, they share the same main functional domains and regulate transcription through the formation of heterodimers with other transcription factors. The absence of an aspartic acid residue in their host cell factor-binding motif (HBM) prevents homodimer formation, ensuring that both isoforms function similarly in transcription regulation (Cockram et al., 2006). Moreover, CREBZF represses the transactivation activity of nuclear receptors on downstream target genes by recruiting histone deacetylases (HDACs) (Xie et al., 2009a). Extensive research has identified CREBZF as a critical regulator of lipid metabolism, with mutations in two single nucleotide polymorphisms (SNPs) within the human CREBZF gene being significantly associated with elevated circulating levels of high-density lipoprotein cholesterol (HDL-C). Additionally, excessive activation of CREBZF has been implicated in accelerating the progression of nonalcoholic fatty liver disease (NAFLD) and nonalcoholic steatohepatitis (NASH) (Ma et al., 2023; Zhang et al., 2018). Our recent research revealed that CREBZF is associated with steroid hormone synthesis. Although conditional knockout of CREBZF in androgen-producing cells does not result in complete infertility in male mice, it significantly reduces testosterone secretion in primary mouse Leydig cells (Lu et al., 2019; Niu et al., 2024). However, the role of CREBZF in female reproductive function remains unknown, and the molecular mechanisms by which CREBZF regulates steroid hormone synthesis are yet to be elucidated.

In this study, we first investigated the reproductive phenotypes and serum levels of relevant steroid hormones in two female mouse models: ovarian-specific CREBZF knockout via in situ AAV9 injection and conditional CREBZF deletion in androgen-producing cells. Forskolin was utilized to enhance steroid synthesis in the NCI-H295R cells, facilitating the validation of CREBZF's function in this process. Transcriptome profiling revealed differentially expressed genes in forskolin-treated cells upon CREBZF knockdown, among which ApoE emerged as a key downstream effector mediating the impact of CREBZF on steroidogenesis. Furthermore, we identified a mechanistic basis whereby CREBZF forms heterodimers with the bZIP transcription factor c-Jun to bidirectionally regulate *Apoe* transcriptional activation. These findings uncover a unique mechanism by which CREBZF regulates the conversion of cholesterol into steroid hormones, providing novel insights into the identification of regulatory factors involved in steroidogenesis.

MATERIALS AND METHODS

Animals

Generation of ovarian CREBZF knockout mice: CREBZF $^{flox/flox}$ mice (C57BL/6) were purchased from Cyagen Biosciences (China). Six-week-old female CREBZF $^{flox/flox}$ mice were randomly assigned to control and experimental groups. Mice were anesthetized using Avertin (30 μL/g body weight) and secured. A small incision was made approximately 2 mm caudal to the last rib on the dorsal side. The ovaries were identified and fixed using blunt forceps, ensuring that the fallopian tubes and blood vessels were not damaged. Recombinant AAV9-Zsgreen and AAV9-Cre-Zsgreen viral vectors were obtained from Hanbio (China), and their titers were verified by quantitative real-time PCR (qRT-PCR). The diluted viral solution (1×10^{11} pfu/mL) was then drawn into a micro-injector connected to a 30G ophthalmic needle, which was carefully inserted into the ovarian stroma for precise delivery. A total of 10 μL of AAV9 was slowly injected into each ovary; control mice received AAV9-Zsgreen, while experimental mice received AAV9-Cre-Zsgreen for conditional knockout. After injection, the ovaries were gently compressed to ensure complete adenovirus penetration and even distribution within the ovarian tissue. The incision was then sutured, and the mice were placed in a warm environment to recover. Mice were allowed a 3-week recovery period following ovarian AAV injection to permit viral infection and plasmid expression. Estrous cycles were monitored continuously for 15 days. One week later, at 12 weeks of age, when all mice were in the non-estrous phase, each mouse was injected with 10 IU of PMSG (Sansheng BioTec, 110914564) to synchronize the estrous cycle. 46 hours after PMSG injection, mice were anesthetized and sacrificed, and serum and necessary tissue samples were collected.

Breeding of CREBZF $^{flox/flox}$, Cyp17a1-Cre^{+} (CREBZF-cKO) female mice: To knock out CREBZF in androgen synthesis cells, Cyp17a1-Cre^{+} mice (Cyagen Biosciences) were crossed with CREBZF $^{flox/flox}$ mice. The resulting CREBZF $^{flox/+}$, Cyp17a1-Cre^{+} (Het) male mice were then mated with CREBZF $^{flox/+}$ or CREBZF $^{flox/flox}$ female mice. Female CREBZF $^{flox/flox}$, Cyp17a1-Cre^{+} mice, designated as CREBZF-cKO, were selected for subsequent experiments, with littermate CREBZF $^{flox/flox}$ females used as controls.

Genotype identification was performed as previously described (Niu et al., 2024). All mice were housed in a specific pathogen-free (SPF) environment with a temperature of 23°C, a 12-hour light/dark cycle, and free access to food. All experimental protocols were approved by the Institutional Animal Care and Use Committee of Northwest A&F University (Approval No. IACUC20240825). Procedures followed the "Regulations for the Management of Laboratory Animals at Northwest A&F University" and the "Guide for the Care and Use of Laboratory Animals" (ISBN-10: 0-309-15396-4).

Dynamic monitoring of the estrous cycle in Mice

The estrous cycle of female mice was dynamically monitored through smear preparation combined with H&E staining. The procedure was performed continuously for 15 days, with operations conducted daily starting at 0800h. A micropipette was used to aspirate 10 μL of sterile physiological saline, which was gently inserted approximately 1 mm into the vaginal opening of the mouse. The saline was then aspirated and ejected three times, followed by evenly spreading the sample onto a glass slide. Once the smear dried, the slide was stained using an H&E staining kit. The slides were examined under a microscope to determine the proportions of different cell types, which were used to identify the stage of the estrous cycle (Byers et al., 2012).

Female mouse reproductive assessment

Adult male CREBZF $^{flox/flox}$ mice with normal fertility were mated with 3-month-old female CREBZF $^{flox/flox}$ or CREBZF-cKO mice at a 1:1 ratio and co-housed continuously for 3 months. The litter size, number of litters, pup survival rate within 7 days postpartum, and total number of surviving offspring over the 3-month period were recorded.

Postpartum pup retrieval test in female mice

To evaluate the impact of conditional CREBZF knockout on maternal behavior and offspring survival, a pup retrieval test (PRT) was employed for behavioral observation and assessment of postpartum female mice (Salais-López et al., 2021; Winters et al., 2022). Three-month-old female mice were individually housed in M5-type cages (294 mm long×195 mm wide×125 mm high). Upon initiation of the trial, a single adult CREBZF $^{flox/flox}$ male, possessing normal fertility, was introduced into the female's cage. The male was removed on day 18 of co-housing to ensure a calm and comfortable environment for parturition. The timing of delivery was meticulously recorded by performing bi-daily checks at 12-hour intervals. The first appearance of pups within 12 h post-birth was designated as postpartum day 0 (PPD0). The detailed protocol for the PRT is outlined below.

Environmental preparation: 1 hour prior to testing, the mother and pups were relocated to a dedicated behavioral testing facility to eliminate potential interference from the original housing environment, including odors and auditory stimuli. The mother was allowed to acclimatize to the new setting.

Isolation and resetting: At the onset of the trial, the mother was briefly transferred to a clean cage for 5 min, during which three randomly selected pups were placed in the farthest corner of the cage, distant from the nest.

Observation and recording: The mother was then returned to the original cage, and her behavior was monitored via a remote camera system integrated with SuperMaze behavioral analysis software (Xinruan Information Technology Co., Ltd, China). The mother’s interactions with the pups were recorded for a 5-minute period, beginning once she made contact with the pups. After each trial, the experimental setup was sanitized with 75% ethanol, and alternating trials were conducted for the control and CREBZF-cKO groups.

Behavioral evaluation: Maternal behavior was analyzed through video recordings and SuperMaze software. The retrieval time for each pup was recorded, with incomplete retrievals logged as 300 seconds. For accurate tracking, the software was calibrated to detect mouse movements with a minimum velocity threshold of 2 cm/s and a sampling frequency of 25 Hz. Detection zones were defined based on a pre-set spatial grid corresponding to the home cage layout. Frame-by-frame motion trajectories were automatically logged, and retrieval was defined by the mouse’s nose-to-pup contact followed by pup transportation back to the nest area. To ensure objectivity and eliminate potential experimenter bias, data collection and analysis were conducted in a double-blind manner. Specifically, all video files were anonymized and randomly coded by a third-party technician prior to analysis. The experimenters conducting behavioral scoring and statistical analysis were unaware of the group identities throughout the entire evaluation process.

Cells culture

The NCI-H295R cell line was purchased from Wuhan Pricella Biotechnology Co.,Ltd. and authenticated by STR profiling. Cells were cultured in DMEM/F12 medium (BasalMedia, China) supplemented with 10% fetal bovine serum (FBS) (Gibco, 10270106), 1% ITS (Insulin-Transferrin-Selenium)-G (Pricella, China), 100 U/mL penicillin, and 100 μg/mL streptomycin. For steroidogenesis induction, NCI-H295R cells were seeded at a density of 3×10^5 cells per well in a 6-well plate. Once the cells adhered and reached approximately 70% confluence, the medium was switched to phenol red-free DMEM/F12 (BasalMedia) to eliminate the weak estrogenic effects of phenol red (De Faria et al., 2016). FBS was replaced with charcoal-stripped calf serum (YOSHI^{TM}, China) to avoid interference from exogenous steroids present in FBS (Tu et al., 2018). Cells were then treated with 10 μmol/L forskolin (FSK) (MCE, HY-15371) for 48 h (Mangelis et al., 2016) or with 1 mmol/L 8-Br-cAMP (MCE, HY-12306A) for 24 h (Sugawara et al., 2006) to stimulate steroid hormone production, and samples were collected for subsequent analysis.

The HEK293T cell line was cultured in DMEM (BasalMedia) supplemented with 10% FBS, 100 U/mL penicillin and 100 μg/mL streptomycin. All the cultures were maintained at 37 °C in a humidified atmosphere containing 5% CO_2.

siRNA transfection

For CREBZF knockdown, siNC or siRNA targeting CREBZF CDS region (Tsingke, China) was dissolved in sterile, nuclease-free ddH_2O. The sequences of both siNC and siCREBZF are listed in Supplementary Table S1. According to the manufacturer's instructions for TurboFect transfection reagent (Thermo Scientific, R0531), the siRNA was pre-incubated in Opti-MEM medium to achieve a final concentration of 50 nM. After a 24-hour incubation period, cells were harvested for Western blot analysis to verify knockdown efficiency. Alternatively, cells were further processed for subsequent experimental procedures.

Quantitative RT-PCR

Total RNA was extracted from NCI-H295R cells and cDNA synthesized using the manufacturer's protocols (Accurate Biology, AG21017; AG11705). qRT-PCR was performed using SYBR Green Pro Taq HS (Accurate Biology, AG11701) on a Bio-Rad CFX96™ Real-Time System. The specific primer sequences used are provided in Supplementary Table S2. Each qRT-PCR reaction was normalized to *Gapdh* expression, and the relative gene expression levels were calculated using the $2^{-\Delta\Delta Ct}$ method.

Western blot analysis

NCI-H295R or HEK293T cells were lysed in ice-cold RIPA buffer for 20 min to extract total protein. The protein concentration was determined using a BCA Protein Assay Kit (Solarbio, PC0020). Protein samples were subjected to SDS-PAGE and transferred to a PVDF membrane (ROCHE, 03010040001). After blocking with 10% non-fat dry milk, the membrane was incubated with the following primary antibodies: CREBZF (1:1000; Proteintech, 19070-1-AP), StAR (1:2000; Proteintech, 12225-1-AP), Cyp11a1 (1:2000; Bioss, bs-3608R), Cyp17a1 (1:2000; Proteintech, 14447-1-AP), Hsd3b2 (1:1000; SantaCruz, sc-100466), c-Jun (1:2000; Zenbio, 380397), p-c-Jun (S63) (1:2000; Zenbio, R22955), ApoE (1:2000; Proteintech, 66830-1-Ig), and β-actin (1:5000; Proteintech, 60009). Following incubation, the membrane was probed with the appropriate HRP-conjugated secondary antibodies (1:5000; Proteintech, SA00001-1/2). Information

regarding the antibodies utilized was showed in Supplementary Table S3. Protein bands were visualized using an ECL substrate and captured on an imaging system (Cytiva, AI800). ImageJ v.1.8.0 software was used for densitometric analysis.

RNA-sequence analysis

NCI-H295R cells were transfected with either siNC or siCREBZF, followed by stimulation with 10 μmol/L FSK for 48 h. Cells were then collected and subjected to RNA-seq, which was performed by Metware Biotechnology Co., Ltd. (China).

RNA was extracted from each sample, and its concentration and integrity were assessed using a Qubit 4.0 Fluorometer (Thermo Fisher, USA) and Qsep400 Bioanalyzer (BiOptic, China), respectively. cDNA libraries were constructed and subjected to quality control before sequencing on the Illumina platform. Raw sequencing data were filtered, and error rate and GC content distribution were examined to obtain clean reads for further analysis. Clean reads were aligned to the reference genome using HISAT2 v.2.1.0 to determine sequence-specific information. Gene expression levels were quantified using FPKM (Fragments Per Kilobase of transcript per Million fragments mapped) to normalize for sequencing depth and transcript length. Principal Component Analysis (PCA) was performed to evaluate dataset characteristics and sample similarity. Differential expression analysis between groups was conducted using DESeq2 v.1.36.0, with multiple hypothesis correction applied to p-values using the Benjamini-Hochberg method to control the False Discovery Rate (FDR). Genes meeting the criteria |fold change|≥1.2 and FDR<0.01 were considered differentially expressed. Gene Ontology (GO), KEGG, and Disease Ontology (DO) enrichment analyses were performed to identify significantly enriched pathways and disease-related terms, providing insights into the biological mechanisms regulated by CREBZF.

Hormone assay

Hormone levels in mice serum and NCI-H295R cell culture supernatants were quantified using enzyme-linked immunosorbent assay (ELISA) according to the manufacturer's protocols for each respective assay kit. The ELISA kits employed included: testosterone (T) (Elabscience, E-OSEL-M0003), estradiol (E_2) (Elabscience, E-OSEL-M0008), corticosterone (CORT) (Cloud-clone, CEA540Ge), oxytocin (OXT) (Cloud-clone, CEB052Ge), and prolactin (PRL) (BNBIT, China).

Intracellular cholesterol content measurement

NCI-H295R cells were seeded in a 6-well plate at a density of 3×10^5 cells per well, with groups including siNC and siCREBZF. After 48 hours of siRNA transfection, cells were harvested using trypsinization, and cell suspensions were collected. The cell number of each sample was determined using a hemocytometer for standardization of cholesterol content measurement. The sample processing procedure was as follows: the cell suspensions were centrifuged at 1 000×*g* for 5 min, and the supernatant was discarded. For each 1×10^6 cells, 1 mL of isopropanol was added, and cells were sonicated in an ice bath for 3 min (power 300 W, 2 s on, 3 s off). The mixture was then centrifuged at 10 000×*g* for 10 min at 4°C and kept on ice until further analysis. Cholesterol content was quantified using total cholesterol (TC) (Solarbio, BC1985) and free cholesterol (FC) (Solarbio, BC1895) assay kits according to the manufacturer's instructions.

Histological analysis

Ovarian samples were fixed in 4% paraformaldehyde and processed using standard histological procedures, including dehydration, paraffin embedding, and sectioning. Paraffin-embedded sections were stained with H&E. Serial sections of the entire ovary were obtained, and follicles were counted based on the presence of an observable oocyte nucleus. The areas of different ovarian regions and follicle diameters were measured using Slide View v.2.5.0 software.

Immunofluorescence

Immunofluorescence staining and microscopic observation were performed on ovarian tissue and NCI-H295R cells. For ovarian tissue, frozen sections were blocked with 5% bovine serum albumin (BSA) (SEVEN, SO110-01) and incubated overnight at 4°C with primary antibodies of CREBZF (1:200; Proteintech, 19070-1-AP) or ApoE (1:300; Proteintech, 66830-1-Ig). The sections were then incubated at room temperature for 1 h with Alexa Fluor™ 594-conjugated secondary antibodies (1:500, ThermoFisher, A-11012; A-11005). Nuclei were stained with DAPI. For the cells, NCI-H295R cells were seeded in 35 mm confocal culture dishes at a density of 1×10^5 cells per well. The cells were treated with 10 μmol/L of FSK for 48 h. After treatment, the culture medium was removed, and the cells were fixed with 4% paraformaldehyde for 15 min. They were then permeabilized with 0.2% Triton X-100 for 30 min, followed by blocking with 5% BSA at room temperature for 1 h. The cells were incubated overnight at 4°C with anti-CREBZF antibody, followed by incubation with fluorescently labeled secondary antibody at room temperature for 1 h, in the dark. The cells were stained with DAPI for nuclear labeling and treated with anti-fade mounting medium. All immunofluorescence samples were photographed using a Leica laser confocal microscope, and fluorescence intensity was analyzed using ImageJ v.1.8.0 software.

Plasmids cloning

The primers used for constructing pcDNA3.1(+)-CREBZF-Flag, pcDNA3.1(+)-c-Jun-HA, pcDNA3.1(+)-ApoE-Myc as well as various truncated and point-mutated fragments of the mouse ApoE promoter, are listed in Supplementary Table S4. The CREBZF, c-Jun and ApoE coding sequences were cloned into the pcDNA3.1(+) expression vector, while promoter fragments and mutants were inserted into the pGL4.10[luc2] basic vector (Promega) for luciferase reporter assays. pRL-CMV (Promega) was co-transfected as an internal control for normalization. All fragments were amplified using PrimeSTAR® GXL DNA Polymerase (Takara, R050Q) and then ligated into the corresponding vectors using a seamless cloning kit (DiNing, DT100-10). All plasmids were verified by Sanger sequencing.

Co-immunoprecipitation (Co-IP)

HEK293T cells were co-transfected with pcDNA3.1-CREBZF-Flag and pcDNA3.1-c-Jun-HA for 48 h and then lysed in cold lysis buffer containing protease inhibitors. After centrifugation, the supernatant was incubated overnight at 4°C with anti-Flag (1:100, TRANS, HT201-01), anti-HA (1:100, Proteintech, 51064-2-AP) antibodies, and control IgG (Proteintech, B900620; Abclonal, AC005). Subsequently, the mixture was incubated with Dynabeads Protein A/G (BEAVER, 22204-5). The immunocomplexes were separated by SDS-PAGE and analyzed by Western blot. The detailed information of antibodies used in this study can be found in Supplementary

Table S3.

Dual-luciferase reporter assay

HEK293T cells were seeded at a density of 5000 cells per well in 24-well culture plates. At 36 h post-transfection, the culture medium was discarded, and 200 μL of cell lysis buffer wasaddedtoeachwell.Thesampleswerethencentrifugedat12000 ×*g* for 5 min at 4°C. The supernatant was carefully collected and transferred to a new brown centrifuge tube, which was placed on ice for subsequent analysis. In accordance with the protocol provided by the Dual-Luciferase Reporter Assay Kit (Beyotime, RG029S), 100 μL of the sample and 100 μL of firefly luciferase reagent were added to each well, and the RLU were immediately measured. Subsequently, 100 μL of Renilla luciferase working solution was added to each well, and RLU readings were recorded again. The firefly luciferase RLU value was normalized by dividing it by the Renilla luciferase RLU value, thus enabling the comparison of reporter gene activation levels across different experimental groups.

Database screening for transcription factor binding targets

The ApoE promoter region (–500 bp, +100 bp) was selected for study, and potential binding sites of c-Jun within this region were predicted using several databases and online tools. (1) JASPAR (https://jaspar.genereg.net/) was utilized, employing its Position Weight Matrix (PWM) for transcription factor binding site (TFBS) prediction. The Homo sapiens species database was selected, and the ApoE promoter sequence was input with a similarity threshold set to 85%. (2) The PROMO tool (http://alggen.lsi.upc.es/), based on the TRANSFAC database, was used to predict binding sites by inputting the sequence and selecting c-Jun as the target transcription factor, with the mismatch threshold set to its default value. (3) The hTFtarget database (https://bioinfo.life.hust.edu.cn/hTFtarget/) was employed, utilizing a dataset of partially experimentally validated data to search for c-Jun's potential regulatory influence on the ApoE promoter region. The results from the three tools were compared, and commonly predicted, highly confident binding regions were selected for further analysis. Specific nucleotide positions of the binding sites, along with their PWM or confidence scores, were recorded for subsequent in-depth exploration.

Electrophoretic Mobility Shift Assay (EMSA)

EMSA was performed to validate the binding of CREBZF and c-Jun to their target sites. Fluorescent probes, competitor probes, and mutant probes were synthesized by Tsingke Biotechnology Co., Ltd. (China), with the primer sequences provided in Supplementary Table S5. HEK293T cells were seeded at a density of 5×10^5 cells per dish in two 60 mm cell culture plates and transfected with 2 μg of pcDNA3.1-CREBZF or pcDNA3.1-c-Jun plasmids, respectively. After 48 hours, the cells were harvested, and nuclear proteins were extracted using the Nuclear Protein Extraction Kit (Beyotime, P0027) following the manufacturer's instructions. In the reaction system, all binding reaction components except for the fluorescently labeled probe were first mixed and incubated at room temperature for 10 min. The fluorescently labeled probe was then added, followed by an additional 20-minute incubation at room temperature. The reaction mixture was loaded onto a 6% EMSA PAGE gel and electrophoresed in an ice bath at 80V for 90 min using 0.5×TBE buffer. Results were captured using the Cy3 channel and recorded via digital imaging.

Statistical analysis

Statistical analyses were performed using GraphPad Prism v.8.0.2 software. The normality of the data distribution was assessed using the Shapiro-Wilk test. For comparisons between two groups, a two-tailed *t*-test was used. For comparisons involving more than two groups, One-way ANOVA was performed. Pairwise comparisons of follicle numbers at different stages of the ovaries were analyzed using multiple *t*-tests with appropriate corrections. Two-way ANOVA was used to compare the activation of different promoter fragments in response to various transcription factor combinations. Ovarian follicle count and fertility data were expressed as the mean±standard deviation (±SD), while all other data were presented as the mean±standard error of the mean (±SEM). Statistical significance was considered when $P<0.05$.

RESULTS

CREBZF deficiency induces ovarian pathological changes and impairs reproductive function

The CREBZF $^{flox/flox}$ mice used for ovarian AAV injection experiments carry LoxP sequences inserted into both alleles, resulting in a single 166 bp PCR product, whereas the WT mice show a 132 bp band (Figure 1A). A schematic of the experimental workflow is shown in Figure 1B. Immunofluorescence staining of ovarian tissue revealed that the Zsgreen fluorescence was present throughout the ovaries of both groups of mice. CREBZF was widely expressed in the ovaries of the control group, particularly in the granulosa cells of atretic follicles and the ovarian stroma, showing stronger positive staining, which is consistent with previous studies. In the AAV9-Cre-Zsgreen group, no positive staining for CREBZF was observed across the ovaries, indicating that Cre recombinase effectively excised CREBZF in the ovaries of the CREBZF $^{flox/flox}$ mice, confirming the successful generation of the CREBZF knockout model (Figure 1C).

The criteria for determining the estrous cycle phases based on H&E-stained smears are shown in Figure 1D. In proestrus, the cell type was primarily nucleated epithelial cells with few anucleate epithelial cells; during estrus, almost all cells were anucleate epithelial cells stained by eosin; in metestrus, white blood cells began to appear; in diestrus, all three types of cells were visible, with sparse epithelial cells and the presence of white blood cells. Mice in the AAV9-Zsgreen group exhibited a regular estrous cycle with normal 4–5 day intervals, while those in the AAV9-Cre-Zsgreen group showed irregular estrous cycles with unregulated repetitions between estrus and diestrus (Figure 1E). Statistical analysis showed a significant reduction in the proportion of mice in proestrus after CREBZF knockout (Figure 1F).

Histological examination revealed that the AAV9-Cre-Zsgreen group exhibited a significantly increased ovarian/body weight ratio (Figure 1G). Observations of the ovaries of knockout mice showed an increased number of atretic follicles with diameters greater than 200 μm. These follicles were characterized by oocyte degeneration, nuclear shrinkage, or the absence of oocytes, with significant granulosa cell apoptosis, reduced or absent follicular fluid, and abnormal

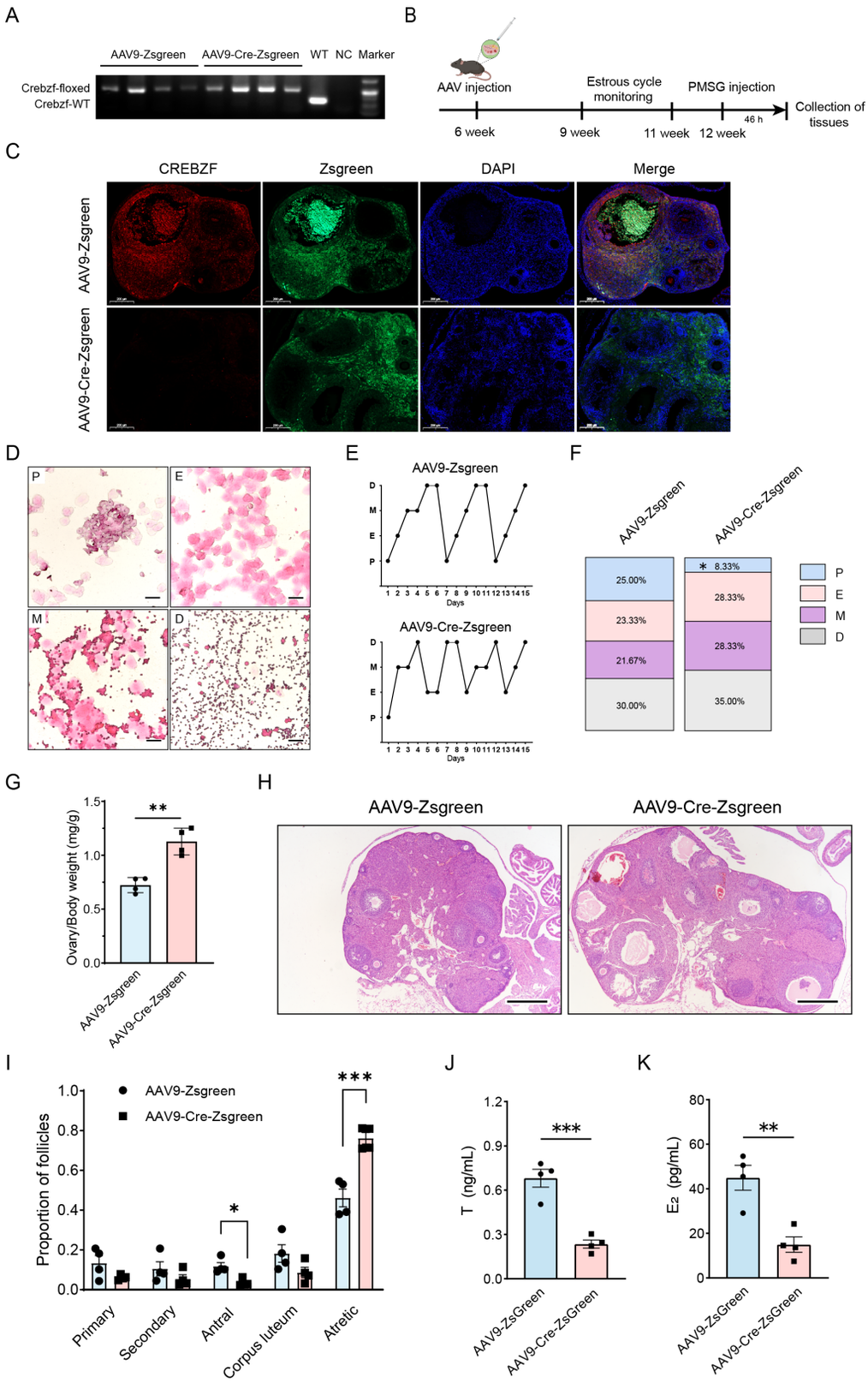

Figure 1 Reproductive phenotype of ovarian CREBZF knockout mice

A: PCR identification of the genotype in CREBZF $^{flox/flox}$ mice. B: Schematic diagram of the experimental procedure. C: Immunofluorescence validation of ovarian CREBZF knockout. Scale bar=200 μm. D: H&E staining of smear preparations from different estrous cycle stages. Scale bar=50 μm. (P: Proestrus; E: Estrus; M: Metestrus; D: Diestrus). E: Representative estrous cycle dynamic curves of the mice. F: Proportional distribution of different estrous cycle stages. G: Statistical analysis of ovarian weight/body weight ratios. H: Representative H&E staining of ovarian tissue sections. Scale bar=500 μm. I: Statistical analysis of follicle distribution at different stages. J: Serum testosterone levels. (T: Testosterone). K: Serum estradiol levels. (E_2: Estradiol). Body weight and percentage of follicles were expressed as mean±SD, and other data were expressed as mean±SEM. n=4 in each group. The P-values were determined by Student's t-test (for G, J and K) or multiple t-tests (for F and I). *: P<0.05, **: P<0.01, ***: P<0.001.

follicular morphology (Figure 1H). Statistical results indicated that the proportion of antral follicles in the AAV9-Cre-Zsgreen group was significantly lower compared to the control group, while the proportion of atretic follicles was significantly higher. No significant differences were observed in the proportions of other follicle stages (Figure 1I). CREBZF knockout in the ovaries impairs both the basic ovarian morphology and follicular development, with compromised antral follicle formation.

Hormone assay results showed that serum levels of testosterone (T) and estradiol (E_2) were significantly lower in the AAV9-Cre-Zsgreen group compared to the control group (Figure 1J, K), indicating that CREBZF knockout impairs sex steroids secretion.

CREBZF knockout in androgen-synthesizing cells reduces T synthesis in female mice during estrous without affecting pregnancy preparation

PCR identification of the CREBZF-cKO mouse genome DNA is shown in Figure 2A. Immunofluorescence analysis of ovarian tissue sections revealed successful CREBZF knockout in the theca cell and a subset of ovarian stromal cells in CREBZF-cKO female mice (Figure 2B), establishing this animal model for investigating the role of CREBZF in androgen-synthesizing cells in female mice. Notably, CREBZF-cKO female mice maintained a complete estrous cycle, with no significant differences in the duration of each

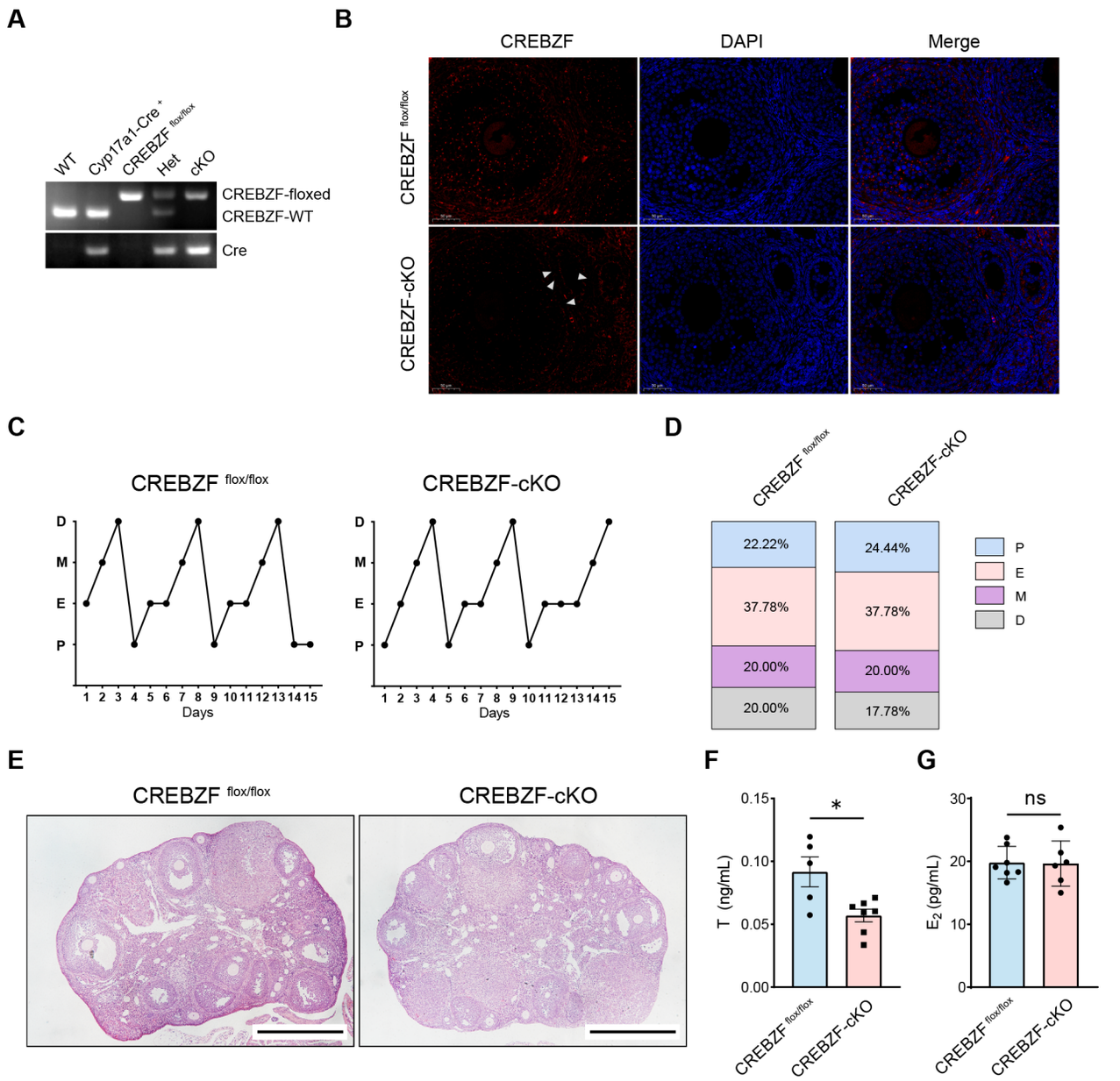

Figure 2 Reproductive phenotypes of CREBZF-cKO female mice

A: PCR genotyping of mice with different genotypes. B: Validation of CREBZF knockout in theca cells and stromal cells. Scale bar=50 μm. (Arrow: Cells with CREBZF knocked out). C: Representative estrous cycle dynamic curves of mice (P: Proestrus; E: Estrus; M: Metestrus; D: Diestrus). D: Statistical analysis of the proportions of each estrous phase. E: Histological analysis of ovarian sections from representative mice. Scale bar=500 μm. F: Serum testosterone levels in 3-month-old estrous female mice. (T: Testosterone). G. Serum estradiol levels. (E_2: Estradiol). Data are presented as mean±SEM. CREBZF $^{flox/flox}$ group n=5–7, CREBZF-cKO group n=6–7. P-values were determined by Student's t-test (for F and G) or multiple t-tests (for D). ns: Not significant. *: P<0.05.

phase compared to control mice (Figure 2C, D). Ovarian morphology during estrus in these mice appeared normal, and follicular development was unaffected, showing no differences from same-litter CREBZF $^{flox/flox}$ mice (Figure 2E). Serum T levels during estrus were significantly reduced in CREBZF-cKO female mice (Figure 2F), while E_2 levels remained unchanged (Figure 2G). These findings indicate that the loss of CREBZF in androgen-synthesizing cells primarily affects testosterone secretion. However, CREBZF in Cyp17a1$^+$ ovarian cells do not appear to be a critical factor in regulating female estrous cycles or follicular development.

Postpartum maternal deficits in CREBZF-cKO females result in impaired offspring survival

Female CREBZF-cKO mice and control females were housed with adult male controls for 3 consecutive months (Figure 3A). Although CREBZF-cKO females were able to conceive and had normal litter sizes (Figure 3B), there were no significant differences in the number of litters produced during the 3-month period (Figure 3C). However, the total number of surviving offspring in CREBZF-cKO females was significantly lower than that in the control group (Figure 3D).

The majority of pup loss in CREBZF-cKO females occurred within the first 7 days postpartum (Figure 3E). Furthermore, CREBZF-cKO mothers exhibited poor maternal care and nursing behavior (Figure 3F). Behavioral tests revealed that in the PRT, as the postpartum days increased, CREBZF $^{flox/flox}$ mothers gradually shortened the time to retrieve pups, showing normal maternal behavior. In contrast, CREBZF-cKO mothers showed significantly longer retrieval times on PPD1, PPD3, and PPD7 compared to controls, with several mothers failing to retrieve pups by PPD7 (Figure 3G).

ELISA results demonstrated that CREBZF-cKO females had reduced serum CORT levels (Figure 3H), significantly increased OXT levels (Figure 3I), and no statistical difference in PRL levels compared to controls (Figure 3J). These findings indicate that the impaired maternal behavior in CREBZF-cKO females is closely associated with the abnormal secretion of corticosterone and oxytocin.

CREBZF regulates steroid synthesis in NCI-H295R cells and affects T and CORT secretion

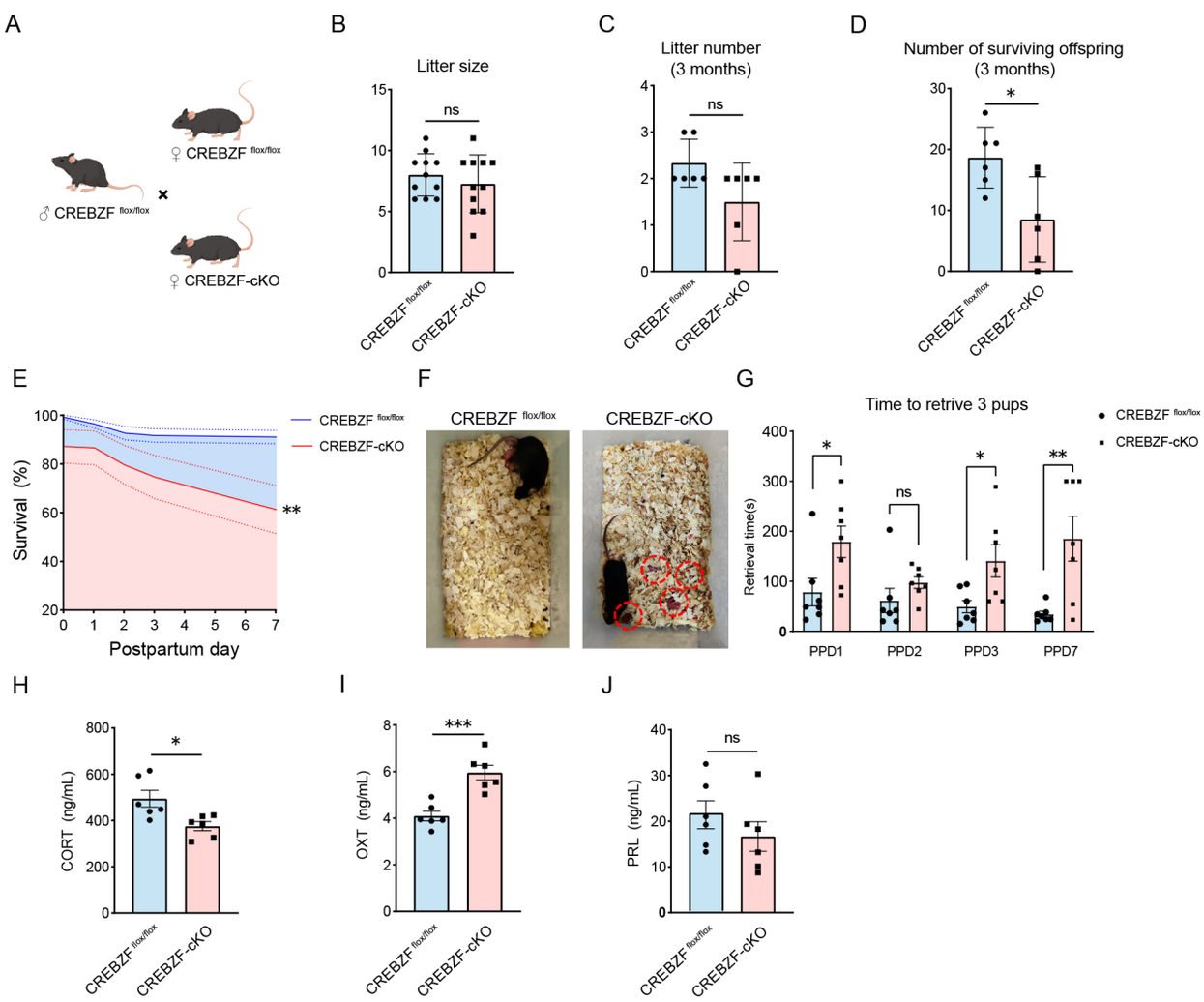

Figure 3 Monitoring of fertility and postpartum maternal behaviors in CREBZF-cKO female mice

A: Mating scheme. B: Litter size. C: Number of litters within 3 months. D: Number of surviving offspring within 3 months. E: Offspring survival curve at day 7 postpartum. F: Representative postpartum behavior of mother mice. G: Statistical analysis of pup retrieval time. H: Serum corticosterone levels in mother mice at 24 h postpartum. (CORT: Corticosterone). I: Serum oxytocin levels. (OXT: Oxytocin). J: Serum prolactin levels. (PRL: Prolactin). Data are presented as mean±SD (B–E) or mean±SEM (G–J). *n*=5–11 in each group. *P*-values were determined by Student's *t*-test (for B–D and H–J) or multiple *t*-tests (for E and G). ns: Not significant. *: P<0.05, **: P<0.01, ***: P<0.001.

After 48 h of FSK treatment, the expression levels of both long and short isoforms of CREBZF were significantly increased in NCI-H295R cells. Concurrently, the expression of key enzymes involved in steroid hormone synthesis, including the rate-limiting enzyme StAR, cytochrome P450 enzymes Cyp11a1 and Cyp17a1, and steroid dehydrogenase 3β-HSD2, was significantly upregulated (Figure 4A, B). Immunofluorescence analysis showed a marked increase in CREBZF-positive staining intensity in both the nucleus and perinuclear cytoplasm following FSK treatment (Figure 4C, D). Direct addition of the cell-permeable 8-Br-cAMP also elevated the expression levels of CREBZF protein (Supplementary Figure S1), indicating that both receptor-dependent and independent pathways induce an upregulation of CREBZF expression in steroidogenesis.

In NCI-H295R cells with CREBZF knockdown (Figure 4E), the secretion levels of T and CORT were significantly reduced (Figure 4F, H), while E_2 levels remained unchanged (Figure 4G).

CREBZF knockdown-induced reduction in T and CORT is not mediated by the classical steroidogenic pathway

To further explore the mechanism by which CREBZF influences steroidogenesis, we investigated the mRNA

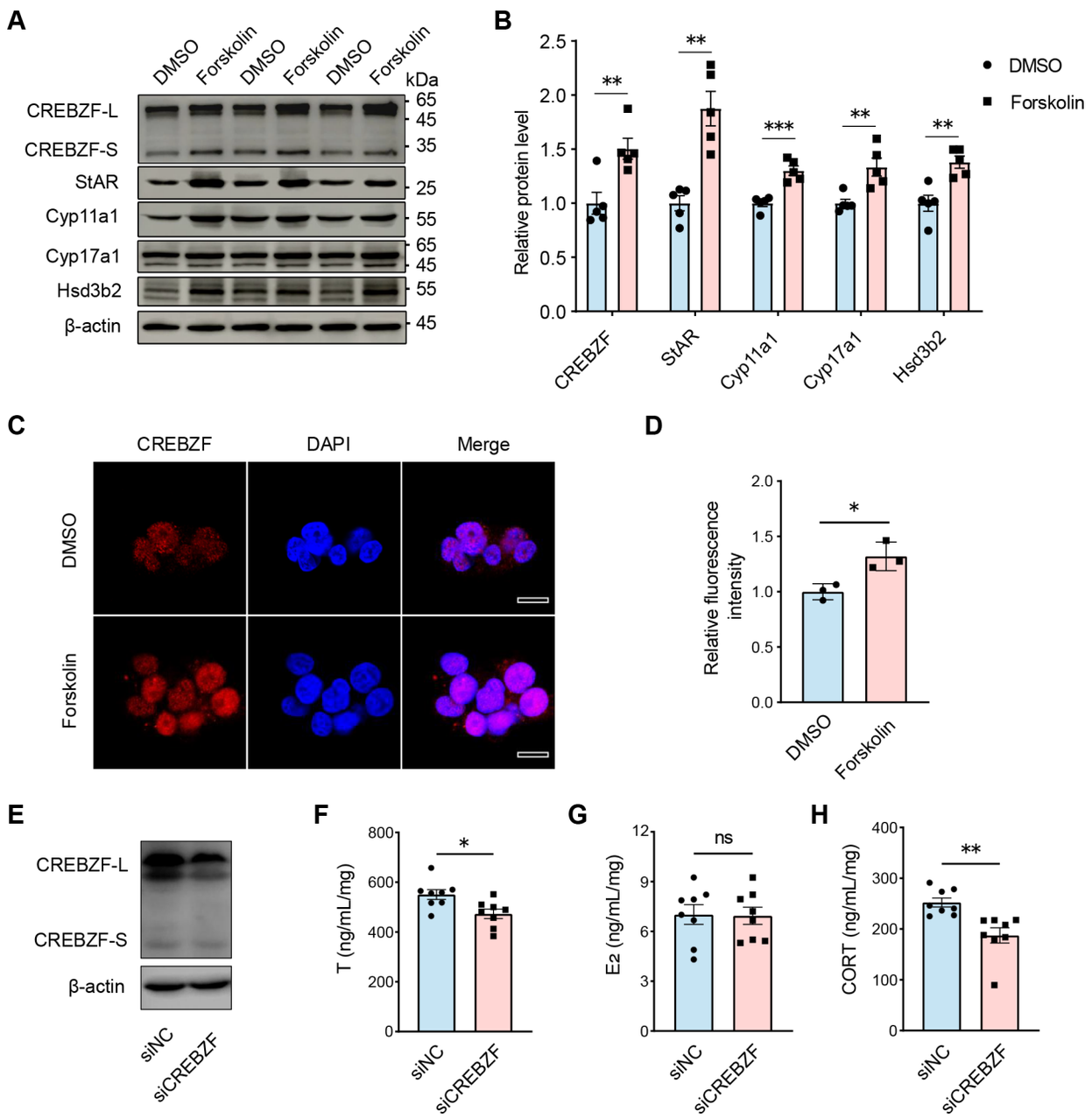

Figure 4 Effect of CREBZF on steroidogenesis in NCI-H295R cells

A: Protein expression of CREBZF and steroidogenic enzymes in NCI-H295R cells stimulated with forskolin for 48 h. B: Western blot grayscale analysis. C: Immunofluorescence staining of CREBZF in cells after forskolin treatment. Scale bar=20 μm. D: Analysis of CREBZF fluorescence intensity. E: Validation of CREBZF knockdown. F–H: Concentrations of testosterone (F), estradiol (G), and corticosterone (H) in the cell supernatants of NCI-H295R cells with CREBZF knockdown after 48-hour forskolin treatment. (T: Testosterone; E_2: estradiol; CORT: Corticosterone); Data are presented as mean±SEM. Each group n≥3. *P*-values were determined by Student's *t*-test. ns: Not significant. *: $P<0.05$, **: $P<0.01$, ***: $P<0.001$.

expression levels of key genes involved in classical steroid hormone synthesis after CREBZF knockdown and FSK induction, using qRT-PCR. The results showed no significant differences in the expression of Star, Cyp11a1, Cyp17a1, Cyp11b1, and Cyp11b2 (Supplementary Figure S2A–F). Interestingly, the expression of Cyp19a1 mRNA was significantly increased (Supplementary Figure S2G). These findings suggest that the reduction in steroids observed upon CREBZF knockdown is likely not mediated by the classical intracellular steroidogenic pathway, and further investigation is needed to uncover the underlying mechanism.

RNA-Seq reveals CREBZF/JUN-ApoE regulate cellular cholesterol levels involved in steroidogenesis

To investigate the global impact of CREBZF knockdown on the cellular mRNA expression profile, RNA-Seq was performed. Principal component analysis (PCA) of the data showed that the first and second principal components (PC1 and PC2) explained the majority of the variation (18.18% and 15.34%, respectively), with clear separation between the si-CREBZF and si-NC groups (Figure 5A). Volcano plot analysis revealed that 32 genes were significantly upregulated and 19 genes were significantly downregulated in the CREBZF knockdown group, with a strong significance in the differential expression of these genes (Figure 5B).

GO analysis identified the top 20 significantly enriched terms, several of which were associated with steroid hormone metabolism and biosynthesis (Figure 5C). KEGG pathway analysis highlighted key biological pathways significantly enriched between the two groups, with several entries related to ovarian steroidogenesis, cortisol, and mineralocorticoid biosynthesis, consistent with previous findings (Figure 5D). DO analysis revealed the potential impact of CREBZF knockdown across multiple disease contexts, with the highest enrichment indices pointing to ovarian-related diseases, suggesting a close association between CREBZF and conditions such as infertility, ovarian dysfunction, and polycystic ovary syndrome (Figure 5E).

A clustering heatmap displayed the top ten most significantly downregulated genes in the si-CREBZF group, including several important genes involved in cellular metabolism and signal transduction. The most downregulated gene was ApoE, a key player in lipid metabolism and steroid transport. Additionally, JUN, encoding the c-Jun protein, was also among the downregulated genes. As c-Jun is a b-ZIP transcription factor like CREBZF, this suggests a potential tight interaction between the two (Figure 5F). qRT-PCR and Western blot analysis confirmed the reduced expression of CREBZF, ApoE, c-Jun, and p-c-Jun at both mRNA (Figure 5G–I) and protein levels (Figure 5J). Immunofluorescence staining demonstrated a reduction in ApoE-positive staining in preantral and antral follicles of ovaries from CREBZF-deficient mice, with no significant difference observed in the corpus luteum (Figure 5M; Supplementary Figure S3).

ApoE is essential for cellular cholesterol transport. To assess whether the decrease in ApoE caused by CREBZF knockdown affects cellular cholesterol metabolism, intracellular total cholesterol and free cholesterol levels were measured in both groups. The results showed a significant reduction in both TC and FC in cells with CREBZF knockdown (Figure 5K, L).

Subsequently, we overexpressed ApoE in CREBZF-knockdown cells and stimulated them with FSK (Figure 5N). The results showed that replenishment of ApoE in both the siNC and CREBZF-knockdown groups increased the secretion of T (Figure 5O) and CORT (Figure 5P). Collectively, these findings suggest that the CREBZF/c-Jun pathway may regulate cholesterol transport through ApoE, influencing cellular steroid hormone biosynthesis.

CREBZF/c-Jun heterodimer binds to different sites in the ApoE promoter to mediate bidirectional regulation

Co-immunoprecipitation (Co-IP) results showed that FLAG-tagged antibodies were used to immunoprecipitate the cell lysates (IP-Flag), and c-Jun-HA was detected in the co-precipitated complex with a molecular weight of approximately 45 kDa by Western blotting (Figure 6A). Reverse immunoprecipitation (IP-HA) with HA antibodies revealed that CREBZF-L and CREBZF-S proteins, with molecular weights of approximately 65 kDa and 35 kDa, respectively, were detected in the c-Jun-HA immunoprecipitate (Figure 6B). No non-specific co-precipitation of CREBZF or c-Jun was observed in the IgG control group. These results confirm the binding interaction between CREBZF and c-Jun.

To explore the activation of the ApoE promoter by CREBZF and c-Jun, a reporter plasmid containing the ApoE promoter region (–2000, +100 bp) was constructed. Dual-luciferase reporter assays showed no significant difference in the activation of the ApoE promoter between the CREBZF overexpression group and the empty vector control. However, overexpression of c-Jun significantly increased the activation of the ApoE promoter, approximately five times higher than the control. Co-transfection of CREBZF and c-Jun resulted in a ten-fold increase in activation, significantly higher than that achieved with c-Jun alone (Figure 6C). These results indicate that c-Jun plays a primary role in regulating ApoE expression, while CREBZF enhances c-Jun-mediated activation of the ApoE promoter.

To further investigate the binding sites of CREBZF/c-Jun, truncated ApoE promoter reporter constructs were generated (Figure 6D). Regardless of whether c-Jun is expressed alone or co-expressed with CREBZF, the luciferase activity in the pGL4.10-ApoE (–2000, +100) group was significantly lower than that in the pGL4.10-ApoE (–2000, 0) group. This suggests that the presence of the region from TSS to +100 bp is unfavorable for the activation effect of CREBZF/c-Jun. In the pGL4.10-ApoE (–2000, 0) group, co-transfection of CREBZF and c-Jun resulted in higher luciferase activity than c-Jun alone. In contrast, in the pGL4.10-ApoE (0, +100) group, CREBZF inhibited luciferase activity, indicating that CREBZF exerts opposing effects on ApoE promoter activation both upstream and downstream of the TSS. Luciferase activity in different truncated fragments within the –2000 to 0 bp region showed no significant differences, indicating that the specific site for c-Jun binding and transcriptional activation lies within the –502 bp to 0 bp region. In the pGL4.10-ApoE (–502, 0) group, CREBZF binding enhanced luciferase activity, suggesting that the CREBZF/c-Jun complex promotes ApoE expression in this region (Figure 6E).

To predict the potential c-Jun binding sites in the –500 to +100 bp region of the ApoE promoter, we used the JASPAR, PROMO, and hTFtarget databases. JASPAR predicted five potential binding sites, PROMO predicted five, and hTFtarget identified three binding sites. The intersection of the three databases identified two novel potential binding sites (Figure 6F). These sites were located at the 5’ and 3’ ends of

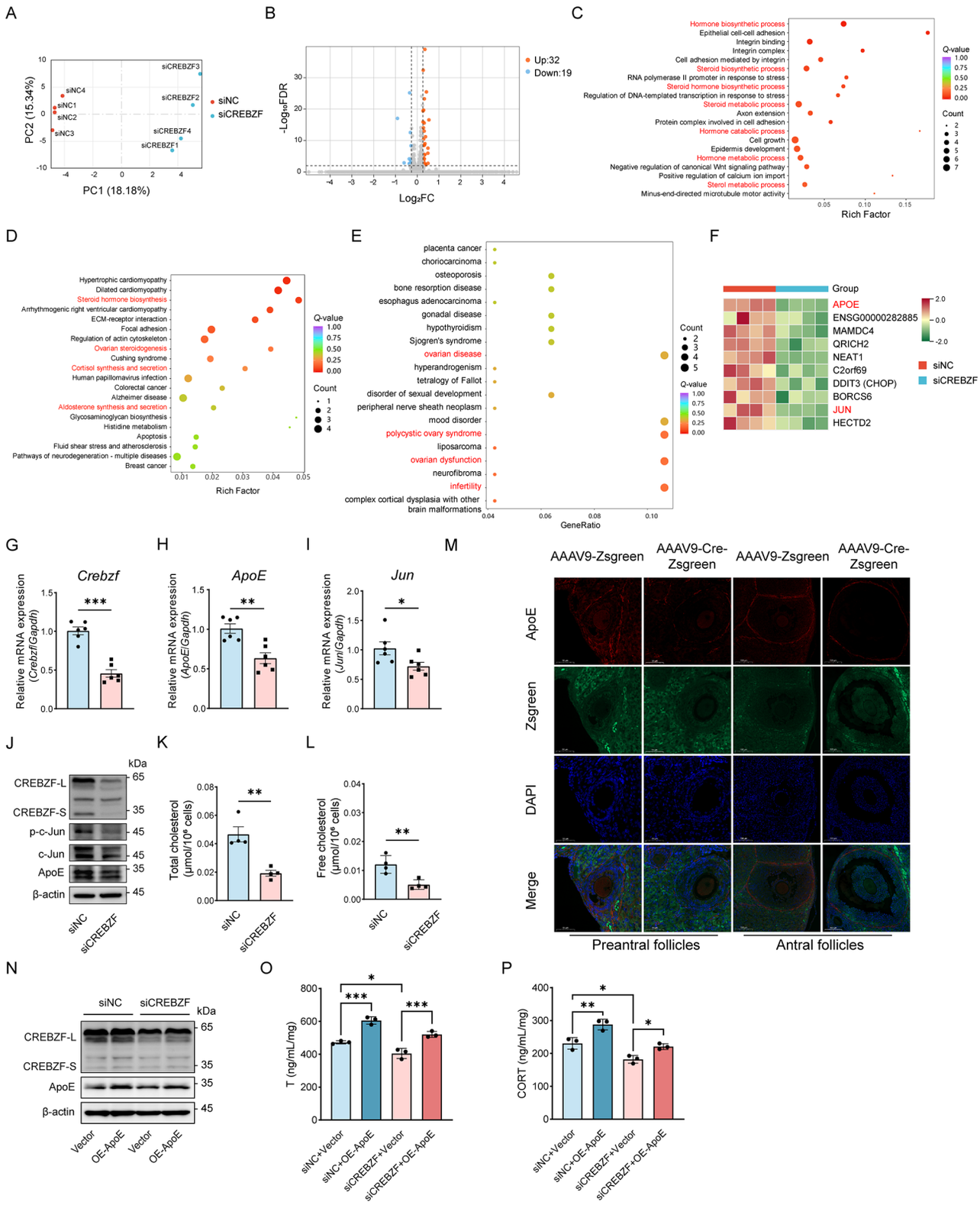

Figure 5 CREBZF knockdown reduces the expression of (p-)c-Jun and ApoE and decreases intracellular steroid content

A: PCA analysis. B: Volcano plot of differentially expressed genes. C: GO analysis of differentially expressed genes. D: KEGG analysis of differentially expressed genes. E: DO analysis of differentially expressed genes. F: Top ten downregulated genes. G–I: qRT-PCR detection of mRNA levels of CREBZF (G), ApoE (H), and c-Jun (I). J: Western blot analysis of CREBZF, c-Jun, p-c-Jun(S63), and ApoE. K: Intracellular cholesterol content. L: Intracellular free cholesterol content. M: Immunofluorescence staining of ApoE in the antral and preantral follicles of ovarian CREBZF knockout mice. Scale bar for preantral follicles: 50 μm; Scale bar for antral follicles: 100 μm. N: CREBZF knockdown and ApoE overexpression detected by Western blot. OE: Overexpression. O: Effect of CREBZF knockdown and ApoE restoration on cell testosterone secretion levels. (T: Testosterone); P: Effect of CREBZF knockdown and ApoE replenishment on cell corticosterone secretion levels. (CORT: Corticosterone); Data are presented as mean±SEM. Each group n≥3. *P*-values were determined by Student's *t*-test. ns: Not significant. *: $P<0.05$, **: $P<0.01$, ***: $P<0.001$.

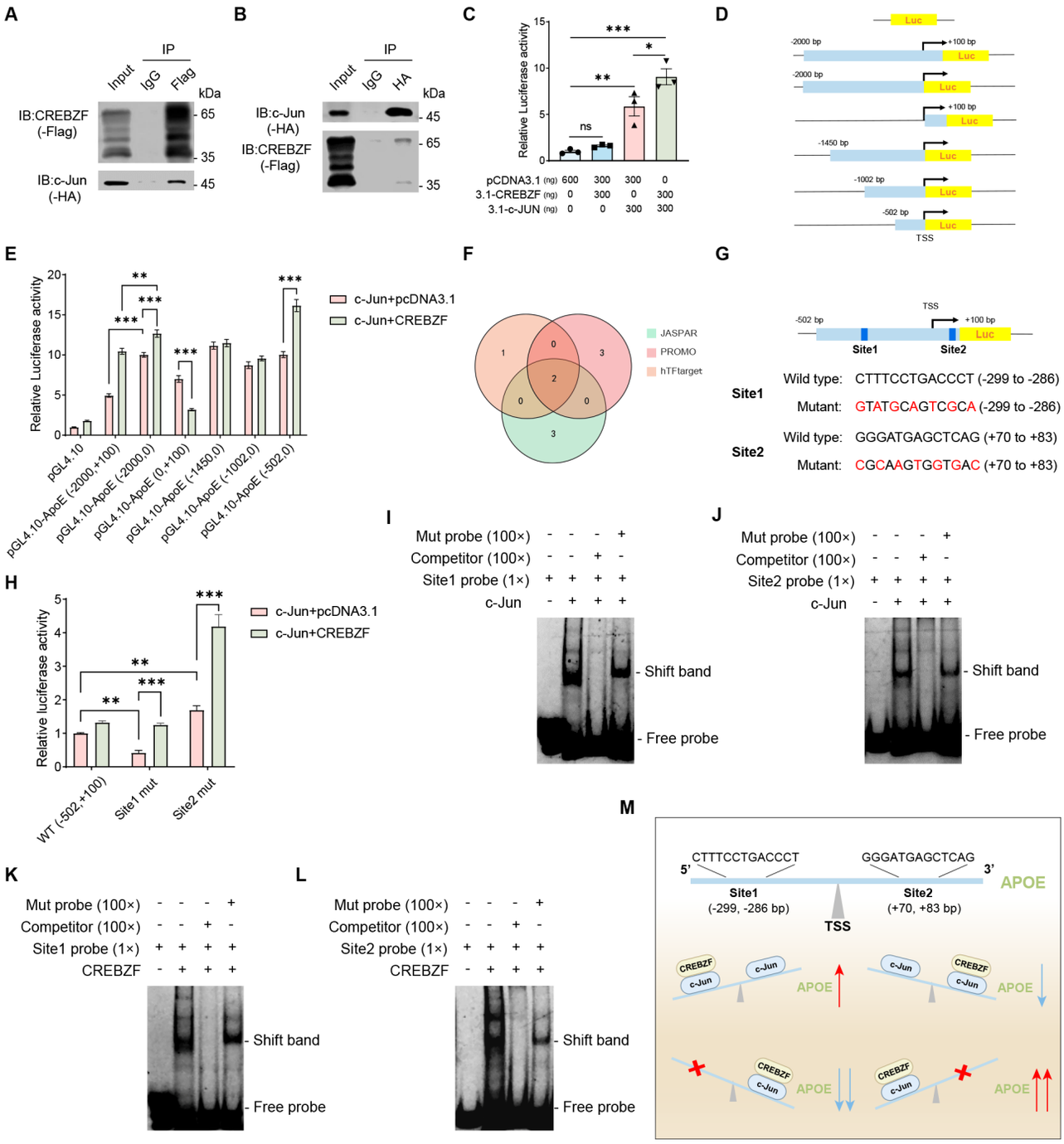

Figure 6 Molecular mechanism of CREBZF/c-Jun regulation of ApoE expression

A: Western blot detection of IP-Flag complexes. B: Western blot detection of IP-HA complexes. C: Dual-luciferase reporter assay validating the activation of the ApoE promoter region (–2000, +100 bp) by CREBZF and c-Jun. D: Schematic diagram of different truncated constructs of the ApoE promoter region for luciferase reporter assays. E: The activation of different truncated regions of the ApoE promoter by CREBZF and c-Jun. F: c-Jun binding sites in the ApoE promoter region (–502, +100 bp) identified by JASPAR, RPOMO, and hTFtarget databases. G: Schematic diagram of mutation luciferase reporter constructs for different binding sites. H: Activation of the ApoE promoter region after mutations at different binding sites by CREBZF and c-Jun. I–L: EMSA validation of c-Jun binding to Site1 (I) and Site2 (J), as well as CREBZF binding to Site1 (K) and Site2 (L). M: Schematic diagram of the mechanism by which CREBZF/c-Jun regulates ApoE expression. Data are presented as mean±SEM. *n*=3 in each group. *P*-values were determined by One-way ANOVA (C) or Two-way ANOVA (E and H). ns: Not significant. *: $P<0.05$, **: $P<0.01$, ***: $P<0.001$.

the TSS and were subsequently mutated (Figure 6G). Mutation of Site1 significantly suppressed c-Jun-mediated transcriptional activation of the ApoE promoter in the –502 to +100 bp region, while mutation of Site2 enhanced c-Jun activation. No matter which binding site is mutated, the presence of CREBZF consistently enhances the transcriptional activation of c-Jun for ApoE (–502, +100 bp) (Figure 6H).

EMSA was further employed to confirm the direct binding of CREBZF and c-Jun to the two predicted sites. The results

demonstrated that both CREBZF and c-Jun bind directly to Site1 and Site2 (Figure 6I–L).

Taken together, CREBZF forms a heterodimer with c-Jun and binds to different sites in the ApoE gene promoter, exerting bidirectional regulation of ApoE expression. Binding of the CREBZF/c-Jun complex to Site1 before the TSS promotes ApoE transcriptional activation, whereas binding to Site2 after the TSS results in significant inhibition of ApoE expression (Figure 6M).

DISCUSSION

The essential role of the ovary in steroid hormone secretion in female animals is well-established. However, the intricate mechanisms regulating ovarian steroidogenesis remain incompletely understood. Research on the function of CREBZF in female reproductive physiology, especially regarding ovarian function and steroid hormone synthesis, is limited, and its precise role remains unclear. To elucidate the function of CREBZF in the mouse ovary, we employed a Cre-loxP tissue-specific gene knockout system. Using surgical techniques, we injected AAV9-Zsgreen/AAV9-Cre-Zsgreen adenoviral vectors into the ovaries of female CREBZF $^{flox/flox}$ mice, establishing a global ovarian CREBZF knockout model. This model enabled preliminary evaluation of the physiological significance of CREBZF expression in ovarian tissue. Notably, AAV9 has demonstrated superior tissue specificity for the ovary compared to other adenoviruses, thus enhancing the efficiency and precision of Cre recombinase delivery. This viral vector system has been widely employed in ovarian disease mechanism studies (Shi et al., 2023; Wang et al., 2023; Zincarelli et al., 2008).

The deletion of ovarian CREBZF markedly reduced serum T and E_2 levels, confirming that CREBZF participates in the regulation of steroid hormone secretion in female animals. Interestingly, despite the substantial reduction in serum steroid hormone levels, the estrous cycle of female knockout mice was not entirely abolished. Knockout mice exhibited a reduced proestrus phase and abnormal fluctuations in the estrous cycle, suggesting that the effects of sex hormones are not solely dependent on serum concentrations, but also on local hormone levels and receptor sensitivities in the ovary, uterus, and other tissues. This phenomenon may be attributable to the complex feedback regulation of the hypothalamic-pituitary-gonadal axis. Histological analysis revealed structural changes in the ovaries of knockout mice. The absence of CREBZF increased the ovarian-to-body weight ratio and decreased the proportion of antral follicles, while the number of follicles larger than 200 μm in diameter increased. Previous studies from our group have demonstrated that CREBZF overactivation promotes granulosa cell apoptosis via the ERK1/2 and mTOR signaling pathways (Chen et al., 2018). This may explain the greater presence of larger follicles in the knockout mice, although this phenomenon did not lead to increased estrogen secretion. Instead, it resulted in follicular atresia of the larger follicles. Ovarian tissue is highly complex, and steroidogenesis is influenced by multiple cell types, including theca cells, granulosa cells, and oocytes, and their interactions (Jones et al., 2024). Thus, the whole-ovary knockout approach may have limitations in fully elucidating the roles of CREBZF in the ovarian steroidogenesis process, as it potentially affects multiple cell types and may induce off-target or indirect effects that confound phenotype interpretation.

The CYP17A1 gene encodes cytochrome P450 17α-hydroxylase/17,20-lyase, which catalyzes the 17α-hydroxylation of pregnenolone or progesterone (P_4), leading to the formation of dehydroepiandrosterone (DHEA) or androstenedione, respectively. This enzyme plays a crucial role in steroid hormone synthesis regulation (Yoshimoto & Auchus, 2015). The Cyp17a1-Cre$^+$ mouse model has been widely used for targeted gene knockout in androgen-synthesizing cells to study steroidogenesis-related phenotypes (Bridges et al., 2008; Fu et al., 2024; Ma et al., 2017). In this study, we crossed Cyp17a1-Cre$^+$ mice with CREBZF $^{flox/flox}$ mice to conditionally knock out CREBZF in the theca cells and ovarian stromal cells. Comparing the effects of this conditional knockout with those of the whole-ovary CREBZF knockout model provided deeper insight into the role of CREBZF in regulating steroid hormone secretion during the female reproductive cycle.

Serum T levels during estrus in the CREBZF-cKO females were reduced as anticipated, consistent with previous findings in male mice (Lu et al., 2019; Niu et al., 2024). This further underscores the central role of CREBZF in regulating sex steroid synthesis, particularly in T synthesis. However, unlike the whole-ovary CREBZF knockout, no significant decrease in serum E_2 levels was observed in the CREBZF-cKO females. This result may explain the absence of overt estrous cycle and ovarian histological abnormalities in these mice. According to the "two-cell, two-gonadotropin" model, E_2 is primarily synthesized by granulosa cells in the ovary (Patel et al., 2009). The knockout of CREBZF specifically in the theca cells may not disrupt granulosa cell function, or the residual T may suffice to maintain estradiol synthesis in granulosa cells. Moreover, E_2 synthesis and metabolic regulation extend beyond the ovarian granulosa cells to other tissues such as the brain, adipose tissue, and liver. T conversion to E_2 likely involves complex compensatory endocrine mechanisms (Pedersen et al., 2004; Rettberg et al., 2014). In addition, CREBZF-cKO females exhibited anxiety-like behavior postpartum, resulting in reduced feeding and pup neglect, which impaired maternal care. To quantify these observations, we performed PRT on postpartum females and found that CREBZF-cKO females had a significantly prolonged pup retrieval time, which contributed to the decreased survival rate of their offspring due to impaired maternal care. Maternal behavior postpartum is primarily influenced by hormones such as corticosterone, oxytocin, and prolactin (Chasseloup et al., 2024; Nishi, 2020; Petersson & Uvnäs-Moberg, 2024). Corticosteroids, including cortisol in humans and corticosterone in rodents, are critical for HPA axis activation and play a pivotal role in perinatal environmental effects. The dynamic balance of corticosterone levels postpartum directly impacts maternal behavior, as well as offspring survival and development (Macrì et al., 2011). Excessive corticosterone levels lead to postpartum depression, resulting in depressive-like behaviors and impaired maternal care. Additionally, overactivation of the offspring's HPA axis and inhibition of the BDNF-mTOR pathway affect emotional and cognitive behavior in adulthood (Xie et al., 2025). However, supplementation with appropriate corticosterone in maternal drinking water during lactation can alleviate anxiety, support maternal behavior, and improve resistance to ischemic neuronal damage, ultimately enhancing offspring learning ability (Catalani et al., 2011). Thus, the reduction of corticosterone levels postpartum in CREBZF-cKO females may directly contribute to their impaired maternal behavior. In addition, the significant

elevation of oxytocin levels in the serum of cKO females may also play a role in the observed maternal behavior deficits. Since both oxytocin and prolactin are peptide hormones, rather than steroids, they were not further explored in this study. Future molecular investigations are required to elucidate the shared and distinct mechanisms by which CREBZF regulates the synthesis of various steroids.

The NCI-H295R cell line, derived from adrenal carcinoma, maintains steroidogenesis capabilities and has been extensively used in steroidogenesis and endocrine research (Rainey et al., 2004; Samandari et al., 2007).Due to the complexity of ovarian theca cells and their variable steroidogenic potential, NCI-H295R cells provide an alternative model, especially since they express high levels of CYP17A1, mimicking the characteristics of theca cells in steroidogenesis-related diseases such as PCOS (Liu et al., 2020; Udhane & Flück, 2016; Vlieghe et al., 2023). In this study, we treated NCI-H295R cells with FSK and 8-Br-cAMP to induce steroidogenesis. Both methods are widely accepted: FSK activates PI3K/Akt and calcium signaling to increase intracellular cAMP, while 8-Br-cAMP directly mimics cAMP activity, stimulating PKA and activating steroidogenic enzymes (Hirsch et al., 2012; Mangelis et al., 2016; Mikhaylova et al., 2008). Regardless of the induction method, CREBZF expression significantly increased, indicating that CREBZF elevation is closely linked to steroidogenesis, independent of AT1 receptor activation. Interestingly, CREBZF knockdown reduced testosterone and corticosterone secretion, while estradiol levels remained unchanged, consistent with the findings in CREBZF-cKO mice. qRT-PCR analysis revealed no significant changes in steroidogenic enzyme expression, except for an unexpected increase in CYP19A1 expression, which converts testosterone to estradiol (Sheng et al., 2024). This increase in CYP19A1 expression may partially explain the unchanged E_2 levels despite reduced T. These results suggest that CREBZF may regulate steroidogenesis through non-classical pathways, highlighting the need for broader gene screening methods, such as transcriptomics.

RNA-Seq analysis revealed a reduction in APOE expression following CREBZF knockdown. ApoE, a critical apolipoprotein involved in lipid transport, is primarily synthesized in the liver, with ovarian and adrenal expression as well (Mahley, 2016; Martínez-Martínez et al., 2020). Recent studies suggest that ovarian ApoE plays a role in follicular development, with ApoE $^{-/-}$ mice exhibiting disrupted cholesterol metabolism, lipid accumulation in the ovaries, and reduced E_2 and P_4 levels (Zhang et al., 2014). Under LH stimulation, theca cells rely on cholesterol-binding lipoproteins for androgen production, and ApoE facilitates the transport of LDL and VLDL into these cells (Oriá et al., 2020). Moderate ApoE concentrations promote androgen synthesis, while excessive ApoE inhibits androstenedione production, underscoring the importance of ApoE-mediated cholesterol transport in steroidogenesis (Zerbinatti et al., 2001). Notably, clinical studies have shown that circulating ApoE-containing lipoprotein is associated with PCOS phenotypes (Fan et al., 2012), and our differential expression analysis revealed enrichment of PCOS-related pathways in the CREBZF knockdown transcriptome. These findings raise the possibility that the CREBZF-ApoE axis may serve as a potential therapeutic target for PCOS.

b-ZIP transcription factors (TFs) are a class of essential transcription factors characterized by a basic DNA-binding domain and a leucine zipper structure. These TFs can form homo- or heterodimers, which specifically recognize and bind to Cis-regulatory elements, thereby modulating the transcriptional activity of downstream genes (Vinson et al., 2002). b-ZIP TFs play significant roles in various cellular processes, including responses to environmental stress, regulation of cell proliferation, and control of programmed cell death. They are also pivotal in immune modulation, metabolic regulation, and cancer development, making them important targets for the prevention and treatment of several diseases (Daenthanasanmak et al., 2022; Lambou et al., 2024). c-Jun, a key member of the b-ZIP family, can interact with other AP-1 family members (e.g., c-Fos, JunB, JunD) to regulate a broad range of biological processes (Li et al., 2024). Recent studies have demonstrated that during estrus and induced superovulation in mice, c-Jun and its family members' expression increases in an LH-dependent manner in granulosa cells (Southall et al., 2025). Prenatal exposure to bisphenol A (BPA) disrupts steroid hormone levels in the placenta, including P_4, E_2, and T, by promoting methylation of the JUN gene (Zhang et al., 2025). Moreover, schisandrin, a major component of Schisandra chinensis, has been identified as a potential therapeutic for PCOS, with bioinformatics analyses indicating that JUN is a key therapeutic target (Dou et al., 2025). In this study, we observed a significant reduction in steroid synthesis upon CREBZF knockdown in NCI-H295R cells, accompanied by a marked decrease in both mRNA and protein levels of c-Jun. These findings highlight a close link between c-Jun and steroidogenesis, and we provide novel evidence that CREBZF may regulate this process by heterodimerizing with c-Jun through its b-ZIP domain to control ApoE transcription and cholesterol transport. Previous research has indicated that high ApoE expression correlates with poor prognosis in colorectal cancer. In HCT116 and HCT8 cells, c-Jun activates ApoE transcription, promoting cancer cell proliferation (He et al., 2023). We observed that c-Jun activates the transcription of the ApoE gene within the region from –2000 bp to +100 bp relative to the TSS. However, the region from the TSS to +100 bp exerted a negative regulatory effect on this process. Among the two c-Jun binding sites we validated, when the CREBZF/c-Jun dimer binds to Site1 (–299, –286 bp), CREBZF enhances c-Jun-mediated transcriptional activation of ApoE. In contrast, binding at the site2(+70, +83 bp) unexpectedly exerted inhibitory effects. EMSA revealed that, like c-Jun, CREBZF directly binds the +70 bp to +83 bp fragment, suggesting potential competitive inhibition between them. Furthermore, as this site lies downstream of the TSS, CREBZF/c-Jun binding could impede the effective assembly of RNA polymerase II and its cofactors. Previous studies have indicated that CREBZF can recruit histone deacetylases (HDACs) (Cui et al., 2024; Xie et al., 2009b), and this deacetylation may reduce the binding of other transcription factors at this site. However, it remains unclear whether the interaction between CREBZF and c-Jun is limited to b-ZIP domain dimerization, or if other proteins serve as intermediaries in this process. Additionally, while this study focused on the full-length CREBZF isoform, it would be valuable to investigate whether the short isoform (CREBZF-S), produced via alternative translation initiation, plays a similar role in this interaction. Moreover, the preference of CREBZF/c-Jun for specific ApoE gene binding sites under different physiological conditions remains unknown and warrants further investigation using advanced techniques.

Although we used the Cyp17a1-Cre^{+} model to achieve targeted deletion, its cell-type specificity is not absolute, and potential off-target effects or incomplete coverage of relevant ovarian cell populations cannot be entirely ruled out. Nonetheless, these findings offer valuable insights into CREBZF's role in female steroidogenesis and ApoE dysfunction regulation in metabolic diseases, with potential applications in gene therapies for reproductive disorders, lipid metabolism abnormalities, atherosclerosis, and cognitive dysfunction.

In summary, CREBZF/c-Jun dimerization regulates the ApoE gene promoter region, exerting bidirectional control. By influencing ApoE-mediated cellular cholesterol transport, CREBZF/c-Jun indirectly modulate steroid hormone synthesis, which is essential for maintaining reproductive physiological functions in female.

DATA AVAILABILITY

The RNA-seq data generated in this study have been deposited in the Genome Sequence Archive (GSA) (https://ngdc.cncb.ac.cn/gsa/) under HRA018802, Science Data Bank (https://www.scidb.cn/c/zoores) under DOI: 10.57760/sciencedb.j00139.00321, and NCBI database (https://www.ncbi.nlm.nih.gov/geo/) under accession numbers GSE334080.

SUPPLEMENTARY DATA

Supplementary data to this article can be found online.

COMPETING INTERESTS

The authors declare that they have no competing interests.

AUTHORS' CONTRIBUTIONS

P.F.L. and Y.P.J. designed the research. H.Y.N., C.L., R.H.Z., M.Z.D. and J.Y.W. performed the research and analyzed the data. H.K.L., Z.H.L. and A.H.W provided technical guidance. H.Y.N. and C. L. wrote the paper. All authors read and approved the final version of the manuscript.

REFERENCES

Bridges PJ, Koo Y, Kang DW, et al. 2008. Generation of *Cyp17i*Cre transgenic mice and their application to conditionally delete estrogen receptor alpha (*Esr1*) from the ovary and testis. *Genesis*, **46**(9): 499–505.

Byers SL, Wiles MV, Dunn SL, et al. 2012. Mouse estrous cycle identification tool and images. *PLoS One*, **7**(4): E35538.

Catalani A, AlemÀ GS, Cinque C, et al. 2011. Maternal corticosterone effects on hypothalamus-pituitary-adrenal axis regulation and behavior of the offspring in rodents. *Neuroscience & Biobehavioral Reviews*, **35**(7): 1502–1517.

Chasseloup F, Bernard V, Chanson P. 2024. Prolactin: structure, receptors, and functions. *Reviews in Endocrine and Metabolic Disorders*, **25**(6): 953–966.

Chen FL, Wen X, Lin PF, et al. 2018. Activation of CREBZF increases cell apoptosis in mouse ovarian granulosa cells by regulating the ERK1/2 and mtor signaling pathways. *International Journal of Molecular Sciences*, **19**(11): 3517.

Cockram GP, Hogan MR, Burnett HF, et al. 2006. Identification and characterization of the DNA-binding properties of a zhangfei homologue in Japanese pufferfish, *Takifugu rubripes*. *Biochemical And Biophysical Research Communications*, **339**(4): 1238–1245.

Connelly MA, Williams DL. 2003. SR-BI and cholesterol uptake into steroidogenic cells. *Trends in Endocrinology & Metabolism*, **14**(10): 467–472.

Cui AY, Xue YQ, Su WT, et al. 2024. Glucose regulation of adipose tissue browning by CBP/P300- and HDAC3-mediated reversible acetylation of CREBZF. *Proceedings of the National Academy of Sciences of the United States of America*, **121**(16): e2318935121.

Daenthanasanmak A, Bamford RN, Yoshioka M, et al. 2022. Triple combination of BET plus PI3K and NF-κB inhibitors exhibit synergistic activity in adult t-cell leukemia/lymphoma. *Blood Advances*, **6**(7): 2346–2360.

Dalhaimer P, Florey B, Isaac S. 2023. Interactions of apolipoproteins with lipid-based nanoparticles. *ACS Nano*, **17**(2): 837–842.

De Faria AN, Zancanela DC, Ramos AP, et al. 2016. Estrogen and phenol red free medium for osteoblast culture: study of the mineralization ability. *Cytotechnology*, **68**(4): 1623–1632.

Dou ZY, Li QX, Zhang J, et al. 2025. Exploring the mechanism of *Schisandra rubriflora* in the treatment of polycystic ovary syndrome based on network pharmacology and molecular docking. *Journal of Ovarian Research*, **18**(1): 16.

Fan P, Liu HW, Wang Y, et al. 2012. Apolipoprotein E-containing HDL-associated platelet-activating factor acetylhydrolase activities and malondialdehyde concentrations in patients with PCOS. *Reproductive Biomedicine Online*, **24**(2): 197–205.

Fu Y, Zhang MJ, Sui BD, et al. 2024. Mesenchymal stem cell-derived apoptotic vesicles ameliorate impaired ovarian folliculogenesis in polycystic ovary syndrome and ovarian aging by targeting WNT signaling. *Theranostics*, **14**(8): 3385–3403.

He LY, Shi MC, Ren SW, et al. 2023. Jun-APOE-LRP1 axis promotes tumor metastasis in colorectal cancer. *Biomolecules & Biomedicine*, **23**(6): 1026–1037.

Helvaci N, Yildiz BO. 2025. Polycystic ovary syndrome as a metabolic disease. *Nature Reviews Endocrinology*, **21**(4): 230–244.

Hirsch A, Hahn D, Kempná P, et al. 2012. Role of AMP-activated protein kinase on steroid hormone biosynthesis in adrenal NCI-H295R cells. *PLoS One*, **7**(1): e30956.

Jones ASK, Hannum DF, Machlin JH, et al. 2024. Cellular atlas of the human ovary using morphologically guided spatial transcriptomics and single-cell sequencing. *Science Advances*, **10**(14): eadm7506.

Lambou K, Tag A, Lassagne A, et al. 2024. The BZIP transcription factor BIP1 of the rice blast fungus is essential for infection and regulates a specific set of appressorium genes. *PLoS Pathogens*, **20**(1): e1011945.

Li F, Tian JQ, Zhang L, et al. 2024. A multi-omics approach to reveal critical mechanisms of activator protein 1 (AP-1). *Biomedicine & Pharmacotherapy*, **178**: 117225.

Liu T, Qin QY, Qu JX, et al. 2020. Where are the theca cells from: the mechanism of theca cells derivation and differentiation. *Chinese Medical Journal*, **133**(14): 1711–1718.

Lu MJ, Zhang RX, Yu T, et al. 2019. CREBZF regulates testosterone production in mouse leydig cells. *Journal of Cellular Physiology*, **234**(12): 22819–22832.

Ma FG, Liu YX, Hu ZM, et al. 2023. Intrahepatic osteopontin signaling by CREBZF defines a checkpoint for steatosis-to-NASH progression. *Hepatology*, **78**(5): 1492–1505.

Ma YP, Andrisse S, Chen Y, et al. 2017. Androgen receptor in the ovary theca cells plays a critical role in androgen-induced reproductive dysfunction. *Endocrinology*, **158**(1): 98–108.

MacrÌ S, Zoratto F, Laviola G. 2011. Early-stress regulates resilience, vulnerability and experimental validity in laboratory rodents through mother-offspring hormonal transfer. *Neuroscience & Biobehavioral Reviews*, **35**(7): 1534–1543.

Maher JY, Gomez-Lobo V, Merke DP. 2023. The management of congenital adrenal hyperplasia during preconception, pregnancy, and postpartum. *Reviews in Endocrine and Metabolic Disorders*, **24**(1): 71–83.

Mahley RW. 2016. Apolipoprotein E: from cardiovascular disease to neurodegenerative disorders. *Journal of Molecular Medicine*, **94**(7): 739–746.

Mangelis A, Dieterich P, Peitzsch M, et al. 2016. Computational analysis of liquid chromatography-tandem mass spectrometric steroid profiling in NCI H295R cells following angiotensin II, forskolin and abiraterone treatment. *The Journal of Steroid Biochemistry and Molecular Biology*, **155**: 67–75.

Martínez-Martínez AB, Torres-Perez E, Devanney N, et al. 2020. Beyond the CNS: the many peripheral roles of APOE. *Neurobiology of Disease*, **138**: 104809.

Mikhaylova IV, Jääskeläinen T, Jääskeläinen J, et al. 2008. Leukemia inhibitory factor as a regulator of steroidogenesis in human NCI-H295R adrenocortical cells. *Journal of Endocrinology*, **199**(3): 435–444.

Miller WL. 2017. Steroidogenesis: unanswered questions. *Trends in Endocrinology & Metabolism*, **28**(11): 771–793.

Miller WL, Auchus RJ. 2011. The molecular biology, biochemistry, and physiology of human steroidogenesis and its disorders. *Endocrine Reviews*, **32**(1): 81–151.

Nishi M. 2020. Effects of early-life stress on the brain and behaviors: implications of early maternal separation in rodents. *International Journal of Molecular Sciences*, **21**(19): 7212.

Niu HY, Li C, Zhang HX, et al. 2024. Androgen synthesis cell-specific CREBZF deficiency alters adrenal cortex steroid secretion and develops behavioral abnormalities in adult male mice. *The FASEB Journal*, **38**(9): e23650.

OriÁ RB, De Almeida JZ, Moreira CN, et al. 2020. Apolipoprotein E effects on mammalian ovarian steroidogenesis and human fertility. *Trends in Endocrinology & Metabolism*, **31**(11): 872–883.

Patel SS, Beshay VE, Escobar JC, et al. 2009. Molecular mechanism for repression of 17α-hydroxylase expression and androstenedione production in granulosa cells. *The Journal of Clinical Endocrinology & Metabolism*, **94**(12): 5163–5168.

Payne AH, Hales DB. 2004. Overview of steroidogenic enzymes in the pathway from cholesterol to active steroid hormones. *Endocrine Reviews*, **25**(6): 947–970.

Pedersen SB, Kristensen K, Hermann PA, et al. 2004. Estrogen controls lipolysis by up-regulating α2a-adrenergic receptors directly in human adipose tissue through the estrogen receptor α. implications for the female fat distribution. *The Journal of Clinical Endocrinology & Metabolism*, **89**(4): 1869–1878.

Petersson M, Uvnäs-Moberg K. 2024. Interactions of oxytocin and dopamine—effects on behavior in health and disease. *Biomedicines*, **12**(11): 2440.

Rainey WE, Saner K, Schimmer BP. 2004. Adrenocortical cell lines. *Molecular and Cellular Endocrinology*, **228**(1-2): 23–38.

Rettberg JR, Yao J, Brinton RD. 2014. Estrogen: a master regulator of bioenergetic systems in the brain and body. *Frontiers in Neuroendocrinology*, **35**(1): 8–30.

Rosenfield RL. 2024. The search for the causes of common hyperandrogenism, 1965 to circa 2015. *Endocrine Reviews*, **45**(4): 553–592.

Salais-López H, Abellán-Álvaro M, Bellés M, et al. 2021. Maternal motivation: exploring the roles of prolactin and pup stimuli. *Neuroendocrinology*, **111**(9): 805–830.

Samandari E, Kempná P, Nuoffer JM, et al. 2007. Human adrenal corticocarcinoma NCI-H295R cells produce more androgens than NCI-H295A cells and differ in 3β-hydroxysteroid dehydrogenase type 2 and 17, 20 lyase activities. *Journal of Endocrinology*, **195**(3): 459–472.

Sheng WM, Wang MM, Li YQ, et al. 2024. Oxidative stress controls lncRNA-mediated sow granulosa cell functions in a FoxO1-dependent manner. *Journal of Animal Science and Biotechnology*, **15**(1): 171.

Shi SJ, Chu GY, Zhang LT, et al. 2023. Deubiquitinase UCHL1 regulates estradiol synthesis by stabilizing voltage-dependent anion channel 2. *Journal of Biological Chemistry*, **299**(11): 105316.

Southall J, Park S, Choi Y, et al. 2025. Granulosa cell expression of fos is critical for regulating ovulatory gene expressions in the mouse ovary. *The FASEB Journal*, **39**(4): e70388.

Sugawara T, Sakuragi N, Minakami H. 2006. CREM confers camp responsiveness in human steroidogenic acute regulatory protein expression in NCI-H295R cells rather than SF-1/Ad4BP. *Journal of Endocrinology*, **191**(1): 327–337.

Touraine P, Chabbert-Buffet N, Plu-Bureau G, et al. 2024. Premature ovarian insufficiency. *Nature Reviews Disease Primers*, **10**(1): 63.

Tu CJ, Fiandalo MV, Pop E, et al. 2018. Proteomic analysis of charcoal-stripped fetal bovine serum reveals changes in the insulin-like growth factor signaling pathway. *Journal of Proteome Research*, **17**(9): 2963–2977.

Udhane SS, Flück CE. 2016. Regulation of human (adrenal) androgen biosynthesis—new insights from novel throughput technology studies. *Biochemical Pharmacology*, **102**: 20–33.

Vinson C, Myakishev M, Acharya A, et al. 2002. Classification of human B-ZIP proteins based on dimerization properties. *Molecular and Cellular Biology*, **22**(18): 6321–6335.

Vlieghe H, Leonel ECR, Asiabi P, et al. 2023. The characterization and therapeutic applications of ovarian theca cells: an update. *Life Sciences*, **317**: 121479.

Wang YC, Ma YD, Liu H, et al. 2023. Hyperandrogen-induced polyol pathway flux increase affects ovarian function in polycystic ovary syndrome via excessive oxidative stress. *Life Sciences*, **313**: 121224.

Winters C, Gorssen W, Ossorio-Salazar VA, et al. 2022. Automated procedure to assess pup retrieval in laboratory mice. *Scientific Reports*, **12**(1): 1663.

Xie HX, Jiang YN, Zhang XM, et al. 2025. Corticosterone-induced postpartum depression induces depression-like behavior and impairs hippocampal neurogenesis in adolescent offspring via HPA axis and BDNF-mtor pathway. *Neurobiology of Stress*, **34**: 100708.

Xie YB, Lee OH, Nedumaran B, et al. 2008. SMILE, a new orphan nuclear receptor shp-interacting protein, regulates SHP-repressed estrogen receptor transactivation. *Biochemical Journal*, **416**(3): 463–473.

Xie YB, Nedumaran B, Choi HS. 2009a. Molecular characterization of SMILE as a novel corepressor of nuclear receptors. *Nucleic Acids Research*, **37**(12): 4100–4115.

Xie YB, Park JH, Kim DK, et al. 2009b. Transcriptional corepressor SMILE recruits SIRT1 to inhibit nuclear receptor estrogen receptor-related receptor γ transactivation. *Journal of Biological Chemistry*, **284**(42): 28762–28774.

Yoshimoto FK, Auchus RJ. 2015. The diverse chemistry of cytochrome P450 17A1 (P450c17, CYP17A1). *The Journal of Steroid Biochemistry and Molecular Biology*, **151**: 52–65.

Zerbinatti CV, Mayer LP, Audet RG, et al. 2001. Apolipoprotein E is a putative autocrine regulator of the rat ovarian theca cell compartment. *Biology of Reproduction*, **64**(4): 1080–1089.

Zhang FF, Hu ZM, Li GP, et al. 2018. Hepatic CREBZF couples insulin to lipogenesis by inhibiting insig activity and contributes to hepatic steatosis in diet-induced insulin-resistant mice. *Hepatology*, **68**(4): 1361–1375.

Zhang SF, Wu QH, He WH, et al. 2025. Bisphenol A alters *JUN* promoter methylation, impairing steroid metabolism in placental cells and linking to sub-representative phenotypes. *Gene*, **941**: 149210.

Zhang T, Dai PY, Cheng D, et al. 2014. Obesity occurring in apolipoprotein E-knockout mice has mild effects on fertility. *Reproduction*, **147**(2): 141–151.

Zincarelli C, Soltys S, Rengo G, et al. 2008. Analysis of AAV serotypes 1–9 mediated gene expression and tropism in mice after systemic injection. *Molecular Therapy*, **16**(6): 1073–1080.